LIGHTWEIGHT UAV PAYLOAD FOR IMAGE SPECTROSCOPY AND ATMOSPHERIC IRRADIANCE MEASUREMENTS

Oliver K. Hasler, Adrian Winter, Dennis D. Langer, Torleiv H. Bryne, Tor Arne Johansen

Norwegian University of Science and Technology (NTNU)
Department of Engineering Cybernetics (ITK)
O. S. Bragstads plass 2D, Elektroblokk D, 7034 Trondheim, Norway

ABSTRACT

This paper presents a low-cost lightweight UAV payload for remote sensing purposes using a small imaging spectrometer made from COTS components. The novel design with an additional upward-facing spectrometer allows for reflectance computation by correcting the push-broom imaging spectrometer data of the ocean surface for different lighting- and atmospheric conditions.

Index Terms— Image spectroscopy, Hyperspectral imaging, downwelling irradiance, ocean color, remote sensing, drone payload

1. INTRODUCTION

The lightweight and compactness of the presented payload allow for conducting long-endurance mapping missions with small aerial drones. The low power consumption and high storage capacity (Sec. 2.3) enable the payload to run continuously with a minimal impact on the performance of even small drones. The payload is a significant improvement when compared to [1, 2], where a similar payload has been presented. The payload was designed for the purpose of ocean color mapping in coastal areas, and includes an upwards pointing spectrometer that can be used to characterize the down-welling light, such that reflectance can be estimated, similar to [3] and other instruments for ocean color. Similar devices have been built by other research groups [4], where atmospheric correction is proposed used radiative transfer modelling.

This paper describes the payload in Sec. 2. The atmospheric correction for different lighting conditions is explained in Sec. 3. Sec. 4 covers the results and conclusion achieved with this payload and Sec. 5 touches on limitations and future improvements.

2. SYSTEM OVERVIEW

The modular architecture of the payload (Sec. 2) comprises of various sensors for remote sensing and navigation purposes. The payload can roughly be divided into three subsystems. The remote sensing sensors, the navigation sensors, and the data processing and storage components.
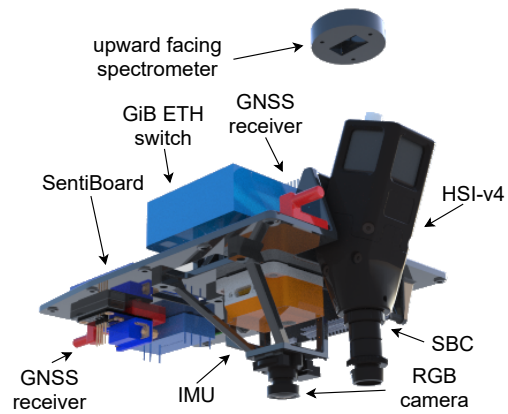

Fig. 1. CAD drawing of Payload

2.1. Optical Sensors

The remote sensing part of the payload consists of three optical sensors. A small lightweight downward-facing push-broom imaging spectrometer (HSI-v4) for ocean color mapping, an upward-facing spectrometer (Hamamatsu C12880MA) to measure downwelling irradiance, and a wide-angle Red-Green-Blue (RGB) camera (Khadas OS08A10 8MP HDR).

2.1.1. Push-broom imaging spectrometer

The downward-facing push-broom imaging spectrometer is described in more detail in [1]. This imaging spectrometer has the advantage of being extremely lightweight (160 g) and being sensitive in the wavelength range necessary to detect e.g. chlorophyll-A (Tab. 1), which is important to map ocean colors and detect algal blooms. The spectrometer was spectrally and radiometrically calibrated according to [5].

Fig. 2 shows an RGB composite of a not georectified imaging spectrometer datacube of Kongsfjorden in Ny-Ålesund/Svalbard (RGB colors are λ_{red} = 630 nm, λ_{green}=550 nm, λ_{blue}=480 nm).

Fig. 2. RGB composite of the hyperspectral datacube, not georectified

2.1.2. Upward facing spectrometer

The most prominent feature of the presented payload is the inclusion of an upward-facing spectrometer. With an additional cosine corrector, this spectrometer can be calibrated to measure down-welling irradiance, which allows to directly calculate the reflectance of the area observed by the imaging spectrometer, independent of lighting and atmospheric conditions. Sec. 3 elaborates further on this. A PIC-24 microcontroller (PIC24FJ128GL306 family) is used as an analog-to-digital converted (ADC). Due to very high sensitivity of the sensor, a set of Neutral Density Filters (NDF) are used to reduce the radiance to the spectrometer and prevent overexposure.

2.1.3. RGB camera

The RGB camera complements the imaging spectrometer with its capability of taking spatial images. This allows using photogrammetry software to get a Digital Elevation Map (DEM) of the overflown area (Fig. 4). Over featureless areas, such as the ocean, techniques such as photogrammetry do not work reliably. Photomosaics can be produced with similar techniques (Fig. 3). Additionally to the function as a remote sensing sensor, the RGB camera can be used as an aiding navigation sensor by incorporating optical flow into the navigation algorithm.

Fig. 3. Photomosaik of the Ny-Ålesund area, overlay over Svalbard Topographical map
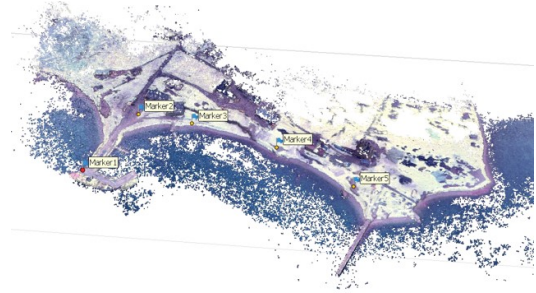

Fig. 4. DEM of the Ny-Ålesund harbor. Produced with Structure from Motion (SfM) technique

2.2. Navigation Sensors

The payload is equipped with a navigation suite consisting of an Inertial Measurement Unit (IMU) from Sensonor (STIM-300) and two Global Navigation Satellite System (GNSS) receivers from u-blox (u-blox ZED-F9P). The IMU is configured to output acceleration and angular velocity measurements at a frequency of 1000 Hz. The GNSS receivers are configured to output raw GNSS observables so that Post-Process Kinematic (PPK) GNSS with a moving-base / rover configuration is possible. These sensors provide data to an IMU/GNSS integrated navigation solution similar to [6].
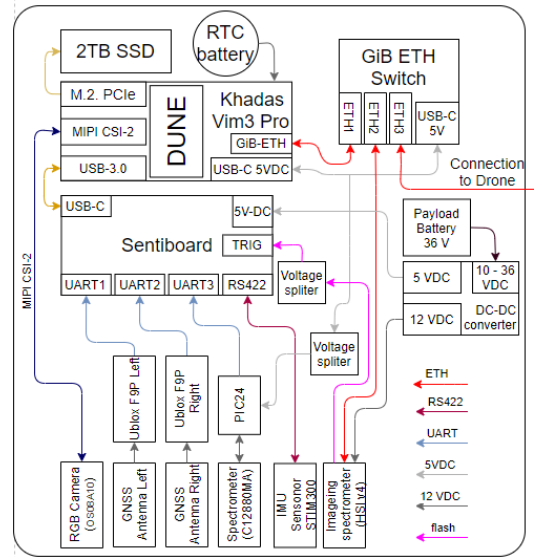

Fig. 5. Schematic overview of the payload architecture

2.3. Data processing and storage

A Single Board Computer (SBC) (Khadas Vim3 Pro) running Ubuntu 20.04.6 LTS forms the central component of the payload. The raw sensor data is stored on a Solid State Drive (SSD) with a storage capacity of 2 TB. A dedicated device (SentiBoard) [7] is used to timestamp all sensor data (except for RGB images) to a precision of 10 ns [7]. These and all other components are schematically shown in Fig. 5.

3. ATMOSPHERIC CORRECTION

Remote Sensing Reflectance $RSR(\lambda)$ is defined in Eq. (1) as the ratio of the upwelling radiance $L_u(\lambda)$ to downwelling irradiance $E_d(\lambda)$. $RSR(\lambda)$ is a material property and is therefore constant for a given material and independent of lighting and atmospheric conditions for nadir pointing [8].

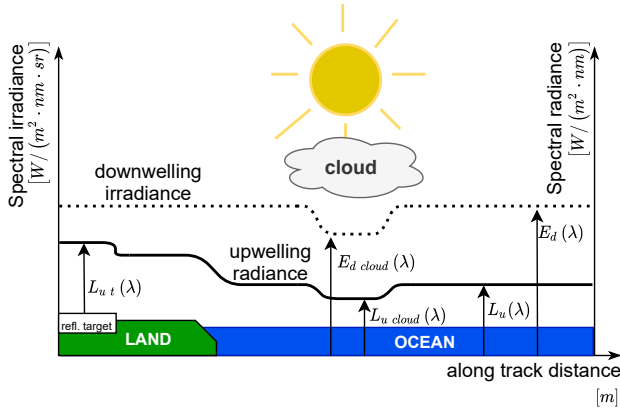$$RSR(\lambda) = \frac{L_u(\lambda)}{E_d(\lambda)} \qquad (1)$$

Fig. 6. Upwelling radiance and downwelling irradiance over different surfaces (left to right, diffuse reflectance target, vegetation/land, water/ocean)

3.1. Mitigation of varying lighting conditions

In airborne imaging spectroscopy remote sensing missions, reflectance is generally calculated as follows:

$$RSR(\lambda) = \frac{L_u(\lambda)}{L_{u\,t}(\lambda)} \cdot \rho_t(\lambda) \qquad (2)$$

$\rho_t(\lambda)$ is the spectral reflectance of a diffuse calibration target, $L_{u\,t}(\lambda)$ is the radiance from the calibration target received at the imaging sensor. One drawback of this approach is the underlying assumption that the lighting conditions remain constant and consistent throughout the entire duration of the mission, including the time the calibration target was overflown. This assumption usually does not hold. A simple example is a cloud, which drastically changes the lighting condition and reduces the downwelling irradiance $E_d(\lambda)$ (see Fig. 6). If reflectance is calculated according to Eq. (2), the measured reflectance $RSR(\lambda)$ changes with the changing downwelling irradiance $E_d(\lambda)$. The concept used in this paper allows us to retrieve $RSR(\lambda)$ independently of lighting conditions. Since the presented payload allows to measure the downwelling irradiance $E_d(\lambda)$ directly, Eq. (1) can be used to calculate the reflectance $RSR(\lambda)$ directly, and independently of any previous measurement. The advantage of this approach can be illustrated with Fig. 6. The ratio of upwelling radiance to downwelling irradiance does not change when the lighting condition change for the upward-facing spectrometer (drone) and the area observed by the imaging spectrometer (e.g. due to flying under a cloud cover).

$$RSR(\lambda) = \frac{L_u(\lambda)}{E_d(\lambda)} = \frac{L_{u\ \text{cloud}}(\lambda)}{E_{d\ \text{cloud}}(\lambda)} \qquad (3)$$

Deriving $RSR(\lambda)$ with Eq. (1), makes a calibration target redundant. Coupled with the payload's direct georeferencing capability, this setup becomes highly suitable for remote sensing missions in remote and inaccessible locations, requiring minimal ground support equipment.

3.2. Calibration

An important part of deriving accurate reflectance $RSR(\lambda)$ with the presented payload is the spectral and radiometric calibration of the push-broom imaging spectrometer (Sec. 2.1.1) and the upward-facing spectrometer (Sec. 2.1.2). The push-broom imaging spectrometer was spectrally and radiometrically calibrated with a calibration procedure based on [5]. The upward-facing spectrometer comes with wavelength calibration coefficients, making a dedicated spectral calibration redundant. The radiometric calibration of the spectrometer was done by calculating the $RSR(\lambda)$ with Eq. (2) over the calibration target, and use Eq. (1) to calculate $E_{d\,t}(\lambda)$. A calibration factor was then derived to scale the signal from the upward-facing spectrometer to fit the calculated signal as closely as possible. This calibration method is inferior to calibration with an integration sphere as shown in [5] and is therefore only used for the proof-of-concept shown in this paper.

4. RESULTS AND CONCLUSION

The presented payload has been used in two field campaigns in Mausund/Norway and in Ny-Ålesund/Svalbard. The data presented in this paper (Figs. 2–4) was gathered during the second field mission in Ny-Ålesund/Svalbard. The method to retrieve $RSR(\lambda)$ data as described in Sec. 3 has been tested in a static test and is presented in the following sections.

4.1. Proof of concept for upward facing spectrometer

The imaging spectrometer was capturing data with a framerate of 18 Hz and the upward-facing spectrometer with a framerate of 20 Hz. Both these sensors have different spectral ranges and a different number of spectral bands (Tab. 1). A matching algorithm was used to assign each imaging spectrometer band the closest wavelength band of the upward-facing spectrometer. A minimal threshold of $\lambda = 3\,\text{nm}$ was used to match bands. Due to the smaller spectral range of the upward-facing spectrometer, the spectral range of the $RSR(\lambda)$ hyperspectral datacube is reduced when the method according to Eq. (1) is used.
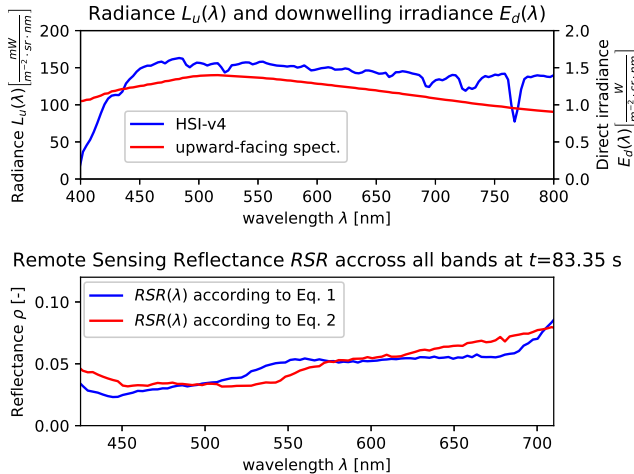
Radiance $L_u(\lambda)$ and downwelling irradiance $E_d(\lambda)$

Remote Sensing Reflectance *RSR* accross all bands at t=83.35 s

Fig. 7. Top part: Radiance (blue) and irradiance (red) measurements. Bottom part: Comparison of reflectance calculated with Eq. (1) (red) and Eq. (2) (blue)

4.2. Comparative Analysis of Reflectance Calculation Methods

The top part of Fig. 7 displays the spectral radiance $L_u(\lambda)$ obtained by the imaging spectrometer for an example pixel (blue) and the spectral downwelling radiance $E_d(\lambda)$ measured by the upward-facing spectrometer (red). The oxygen absorption band at $\lambda \approx 770\,\mathrm{nm}$ is not visible for the upward-facing spectrometer, due to the large spectral resolution of that sensor (Tab. 1). In the bottom part of Fig. 7 the $RSR(\lambda)$ calculated with Eq. (1) (red) and Eq. (2) (blue) is shown. The spectrometer was calibrated as described in Sec. 3.2. A white mat paper which was not further characterized was used as a calibration target, $\rho_t = 0.82$ across all wavelengths has been assumed. This calibration method may result in imprecision due to the unknown lighting conditions and variations in the reflectance across all bands. This is one of the reasons identified for the mismatch between the reflectance calculated with Eq. (1) and Eq. (2).

4.3. Discussion

The results presented here are a proof-of-concept, demonstrating the potential of the presented payload to generate a hyperspectral $RSR(\lambda)$ datacube without additional ground equipment. The next phase involves the generation of a $RSR(\lambda)$ datacube under different lighting conditions before the concept will be proven with further flight tests.

5. LIMITATIONS AND FUTURE IMPROVEMENTS

Besides the issues regarding the imaging spectroscopy equipment raised in Sec. 4, there are a few other limitations which could be improved.

Table 1. Spectral ranges and resolutions

Sensor	Spectral Range [nm]	Spectral Resolution FWHM [nm]
HSI-v4	400.0 - 800.0	3.6
C12880	310.0 - 879.0	12.0
SpectraPen L50	340.0 - 790.0	7.0

- Using a spectrometer with a higher spectral resolution and a higher spectral range would improve the reflectance calculation according to Eq. (1) significantly.
- The imaging spectrometer used has a rather narrow fov of 10.61°. This could be improved with a horizontally built-in camera and convex mirror, or a wider slit.
- A cosine corrector (resp. optical diffuser) on the upward-facing spectrometer would allow calibrating this sensor for global irradiance measurements.

6. ACKNOWLEDGEMENTS

7. REFERENCES

[1] Fred Sigernes et al., "Do it yourself hyperspectral imager for handheld to airborne operations," *Optical Express*, 2018.

[2] João Fortuna and Tor Arne Johansen, "A lightweight payload for hyperspectral remote sensing using small uavs," in *WHISPERS 2018*, 2018, pp. 1–5.

[3] K. Nordkvist, "Ocean color retrieval using dronespex a miniature imaging spectrometer," M.S. thesis, Luelå University of Technology, 2008.

[4] Yiwei Mao et al., "Openhsi: A complete open-source hyperspectral imaging solution for everyone," *Remote Sensing*, vol. 14, no. 9, 2022.

[5] Marie Bøe Henriksen et al., "Pre-launch calibration of the hypso-1 cubesat hyperspectral imager," in *2022 IEEE Aerospace Conference (AERO)*, 2022, pp. 1–9.

[6] Oliver Hasler et al., "Direct georeferencing for hyperspectral imaging of ocean surface," in *2023 IEEE Aerospace Conference*, 2023, pp. 1–19.

[7] Sigurd M. Albrektsen and Tor Arne Johansen, "User-configurable timing and navigation for uavs," *Sensors (Basel, Switzerland)*, vol. 18, no. 30061522, pp. 2468, July 2018.

[8] Michael T.Eismann, *Hyperspectral Remote Sensing*, SPIE Press, 2012.